P-WAVE AND S-WAVE ANGLE DEPENDENT VELOCITY PREDICTION THROUGH PRESSURE-DEPENDENT COMPLIANCE COMPONENTS

Qi Ren

Department of Geological Sciences
The University of Texas at Austin

ABSTRACT

Worldwide interest in shale as a hydrocarbon resource requires new approaches to reservoir characterization. Due to its intrinsic anisotropic properties (commonly VTI), the existing isotropic rock physics models are no longer suitable in shale studies. Therefore, it is important to utilize anisotropic rock physics models for shale in further research. These anisotropic models should account for the phase velocity with non-zero propagation angles with respect to the reference frame. My work was aimed at developing a feasible method to predict angle-dependent velocities (P, SH and SV) in a VTI system. In such an anisotropic system, wave velocities are determined by the elastic tensor with five independent components. The well data I used was from the Haynesville Shale, core samples from this well, and an analogous hard shale sample. The model used to describe the VTI system treats the compliance tensor components as an exponential function of effective pressure. I built an integrated workflow to model the compliance tensor from stress-dependent vertical P-wave velocity lab measurements and then predicted the velocities. Then I used the log data and analogous shale data to estimate the uncertainty. The difference between well log and modeled P-wave results at a test location was 3%. The modeled P-wave results fell between 10% uncertainty estimates over the range of propagation angles. For the S-wave, the difference was much larger, but they showed the same angle-dependent variation trends. The large difference can be associated with both improper use of analogous shale data and the lack of measurements. Therefore, the analogous data was required to provide reliable S-wave velocity. Applying these results to field seismic data, we could reliably predict the angle-dependent P-wave velocity at the seismic scale.

INTRODUCTION

With the rapid growth of interest in natural gas production from shale formation, seismic based shale related research becomes more necessary for reservoir characterization away from borehole measurements. Although shale (mudstone) forms approximately 70% of sedimentary rock, much remains to be studied (Hart, 2011). For Example: How does kerogen affect anisotropy of shale (Vernik, 1990)? How are organic-rich shales best characterized (Vanorio et

al., 2008)? A big challenge for shale research is that these rocks can exhibit large intrinsic anisotropy. Typically they are assumed to have vertical transverse isotropy (VTI), due to aligned microscopic clay platelets (Jones, 1981; Vernik and Nur, 1992). Isotropic rock physics models as applied to conventional reservoirs are not sufficient for describing shale properties. Therefore, it is important to utilize anisotropic rock physics models for shale in further research. These anisotropic models should account for the phase velocity with non-zero propagation angles with respect to the reference frame. It will be very helpful if the angle-dependent velocities could be predicted from a just a few measurements, which is the basis of this work.

In VTI media, the angle-dependent velocities are determined by five independent elastic components. These components are extremely difficult to measure in some cases. Wang (2002) measured the five stiffness components of 17 shale samples at different pressures. For most shale formations, these five elastic components are unknown. Pervukhina et al. (2011) developed a model for TI media that describes the system in terms of pressure-dependent compliance components. Advanced to previous work (Ciz and Shapiro, 2009), the Pervukhina approach requires two fewer parameters. By this model, one can predict the last two compliance components with three of the other pressure-dependent components available. However, having three pressure-dependent compliance components series is still uncommon for most shale cases.

In this paper, we present an integrated method to model the elastic components and then predicted the velocities for a dataset from the Haynesville Shale from an insufficient number of measurements. The data used was pressure-dependent vertical P-wave velocity lab measurements and analogous shale measurements from Wang (2002). The rock physics model used was Pervukhina pressure-dependent TI model. The uncertainty of predicted velocities was estimated by log data from the Haynesville Shale and the analogous shale data.

METHODOLOGY AND DATA

VTI media

Seismic waves propagate through VTI shale in 3 modes: P-wave, horizontally polarized S-wave (SH), and vertically polarized S-wave (SV). Shale is modeled as VTI media as shown in Figure 1. The propagation velocities are determined by the stiffness tensor (**C**) with 5 independent components (C_{11}, C_{33}, C_{44}, C_{66} and C_{13}), and are calculated through Equations 1–4 (Mavko et al., 2009). Here, θ is the angle between the propagating direction and 3-axis. These five components correspond to Vp-0°/45°/90°, Vsh-0°/90° measurements that rarely are all measured. Therefore, the key issue for the project is modeling the stiffness tensor with insufficient measurements.

$$V_P = \left(C_{11}(\sin\theta)^2 + C_{33}(\cos\theta)^2 + C_{44} + \sqrt{M}\right)^{1/2}(2\rho)^{-1/2}, \tag{1}$$

$$V_{SV} = \left(C_{11}(\sin\theta)^2 + C_{33}(\cos\theta)^2 + C_{44} - \sqrt{M}\right)^{1/2}(2\rho)^{-1/2}, \tag{2}$$

$$V_{SH} = \left(C_{66}(\sin\theta)^2 + C_{44}(\cos\theta)^2/\rho\right)^{1/2}, \tag{3}$$

$$M = [(C_{11}-C_{44})(\sin\theta)^2 - (C_{33}-C_{44})(\cos\theta)^2]^2 + \left(C_{13}+C_{44}\right)^2(\sin 2\theta)^2 \tag{4}$$
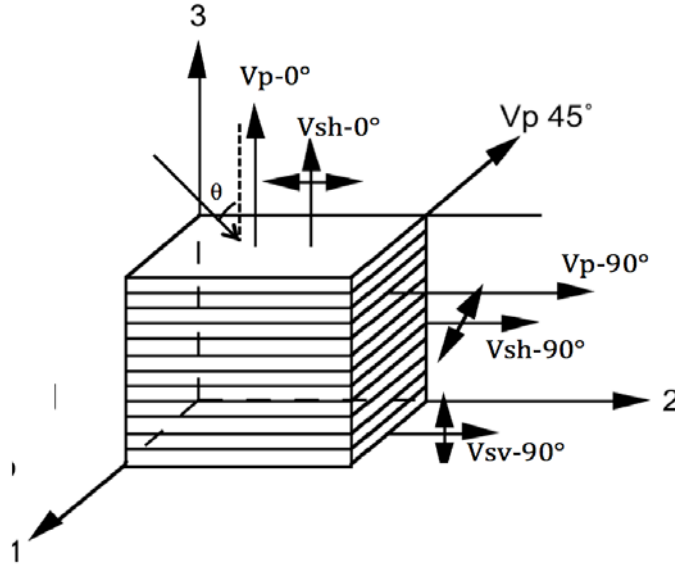

Figure 1. VTI system and propagated waves (Podio, 1968).

Rock physics model and procedure

The Pervukhina model describes the compliance components as an exponential function of effective pressure. These functions are presented in Equations 13–17. S_{ij}^0 in these equations are required at high pressure when all compliant cracks are supposed to be closed. Four coefficients (SnBt, B, Pc and η) are 1) the specific tangential compliance B_T; 2) the ratio $B=B_N/B_T$, where B_N is the specific normal compliance; 3) the characteristic crack closing pressure Pc; and 4) the crack orientation anisotropy parameter η. S_nB_T is the tangential compliance of an individual crack per unit area multiplied by the normalized specific surface area of cracks per unit volume.

$$\Delta S_{11} \equiv S_{11} - S_{11}^0 = S_nB_T \exp(-P/P_c) \times (14 + 4\eta + 21B + 3B\eta)/105, \tag{5}$$

$$\Delta S_{33} \equiv S_{33} - S_{33}^0 = S_nB_T \exp(-P/P_c) \times (14 + 6\eta + 21B + 15B\eta)/105, \tag{6}$$

$$\Delta S_{44} \equiv S_{44} - S_{44}^0 = S_n B_T \exp(-P/P_c) \times (42 + 16\eta + 28B + 12B\eta)/105, \qquad (7)$$

$$\Delta S_{66} \equiv S_{66} - S_{66}^0 = S_n B_T \exp(-P/P_c) \times (42 + 10\eta + 28B + 4B\eta)/105, \qquad (8)$$

$$\Delta S_{13} \equiv S_{13} - S_{13}^0 = S_n B_T \exp(-P/P_c) \times (-7 - 3\eta + 7B + 3B\eta)/105. \qquad (9)$$

In the Pervukhina approach, Equations 5–9 are over-determined when more than three pressure-dependent compliance components are available. The Levenberg-Marquardt non-linear fitting method (Pervukhina, 2011; More, 1997) was applied to solving these four coefficients. The fitting procedure is shown in Figure 2.
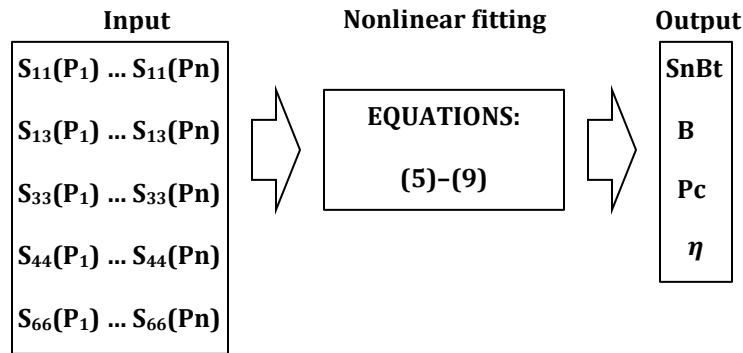
Figure 2. Fitting procedure for solving coefficients in the Pervukhina et al. (2011) model.

However, the data set from Haynesville Shale did not have enough measurements to calculate any compliance components using this model. As analogous data, we used the hard shale pressure-dependent elastic measurements from Wang (sample G3, 2002) to build an initial model. The measurements are listed in Table 1. They are in terms of stiffness components. From Equations 10–14, these stiffness components were converted to compliance components. The fitting procedure was the same as in Figure 2.

Table 1. Measured properties of the G3 hard shale sample from Wang (2002). The density of this sample is 2.560 g/cm3 and porosity is 6.7%.

Effective Pressure MPa	C_{11} GPa	C_{44} GPa	C_{13} GPa	C_{33} GPa	C_{66} GPa	ε	γ	δ
20.69	54.42	14.73	7.94	36.18	20.23	0.297	0.182	0.116
34.48	55.32	14.95	8.35	37.40	20.36	0.265	0.180	0.099
44.82	56.09	15.12	8.71	38.40	20.48	0.240	0.177	0.095
55.17	56.98	15.34	9.30	39.67	20.63	0.217	0.175	0.106

$$S_{11} + S_{12} = C_{33}/[C_{33}(C_{11} + C_{12}) - 2C_{13}^2], \tag{10}$$

$$S_{11} - S_{12} = 1/(C_{11} - C_{12}), \tag{11}$$

$$S_{13} = -C_{13}/[C_{33}(C_{11} + C_{12}) - 2C_{13}^2], \tag{12}$$

$$S_{33}(C_{11} + C_{12})/[C_{33}(C_{11} + C_{12}) - 2C_{13}^2], \tag{13}$$

$$S_{44} = 1/C_{44} \tag{14}$$

$$C_{11} + C_{12} = S_{33}/[S_{33}(S_{11} + S_{12}) - 2S_{13}^2], \tag{15}$$

$$C_{11} - C_{12} = 1/(S_{11} - S_{12}), \tag{16}$$

$$C_{13} = -S_{13}/[S_{33}(S_{11} + S_{12}) - 2S_{13}^2], \tag{17}$$

$$C_{33} = (S_{11} + S_{12})/[S_{33}(S_{11} + S_{12}) - 2S_{13}^2], \tag{18}$$

$$C_{44} = 1/S_{44} \tag{19}$$

Then we modified the initial model to fit the Haynesville Shale lab measurements. This modification consisted of using the anisotropy parameters from the analogous shale as a proxy for the Haynesville Shale. Both the model and analogous hard shale data were brine saturated whereas the lab data was measured on dry rocks. Thus, fluid substitution was required before further analysis. The modified procedure is shown in Figure 3. This integrated procedure enabled TI system velocity prediction, even from highly insufficient measurements.
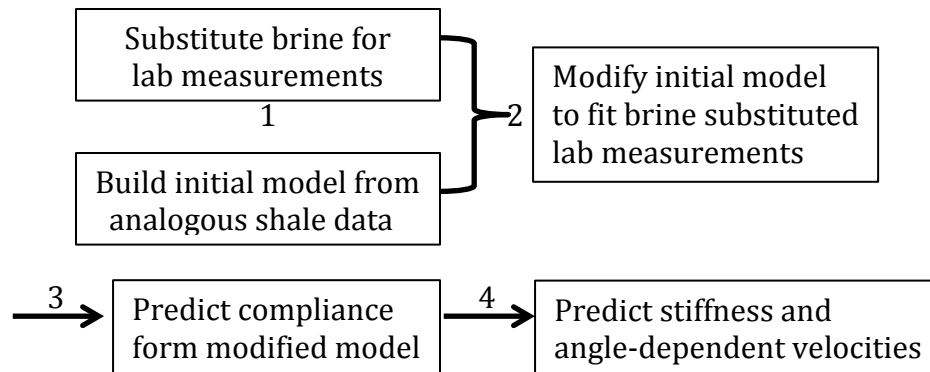
Figure 3. Integrated procedure for velocity prediction. The initial model was built (Step 1) by the same procedure shown in Figure 2. The pressure-dependent elastic components used for initial model was hard shale sample (G3) from Wang (2002). The compliance tensor resulted from step 3 was converted back to stiffness in step 4 by Equations 15–19, and velocities were calculated by Equations 1–4.

Case study

The case study was from Haynesville shale in east Texas. This formation is relatively thick, organic rich shale, which deposited in shallow marine environment during late Jurassic period (Hammes et al., 2011). The Haynesville is assumed to be a typical VTI system with high anisotropy and is highly over-pressured. We had pressure-dependent lab measurements of vertical P-wave velocity on dry samples from two different depths (depth 1 and depth 2) in a single well (Figure 4). Depth 1 was 40ft shallower than depth 2. The highest velocity was around 3300m/s at 50MPa. Also, we had velocity log of P and S wave in the same well and the analogous hard shale data (sample G3 from Wang, 2002). The core sample XRD showed that the lithology was 30% quartz, 30% calcite, 30% clay, 5% kerogen and 5% others. I assumed that the study area was homogenous in terms of lithology.
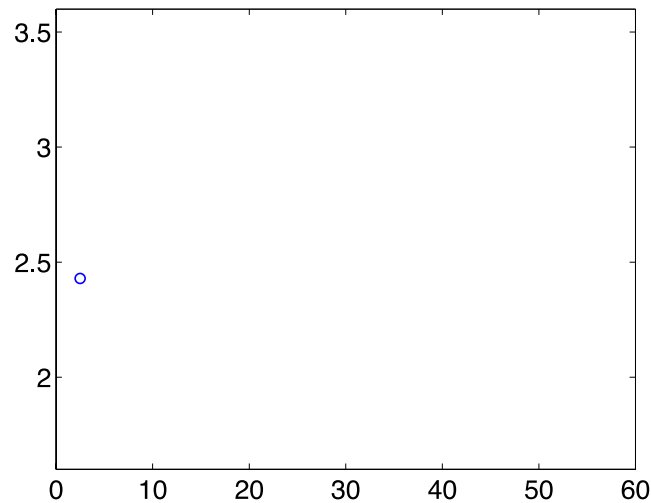
Figure 4. Haynesville Shale data: dry measured P-wave velocity Versus effective pressure. The large differences at low pressure is indicative of the fact that core plugs were dried and desiccated due to long-term storage in a unpreserved state.

RESULTS

Initial model

By the procedure shown in Figure 2, the initial model based on G3 sample (Wang, 2002) was built as the first step. With all the five compliance components at four different pressure and the

S_{ij}^{0} the as input, we obtained a system of twenty equations and four unknown parameters. The Marquardt-Levenberg schemed was used to fit these over-determined equations. Table 2 contains the best fitting parameters and the S_{ij}^{0} used as input. Figure 5a shows the modeled pressure-dependent compliance components. The difference between the model and the measurements is almost negligible. With this initial model, we could predict the compliance components of the G3 sample at any pressure and calculate the stiffness components and velocities. Figure 5b shows the comparison of pressure-dependent velocities between the modeled results and measured data at zero degree. There is only one set of S-wave because SV and SH- wave velocities are the same at zero degree. The modeled velocities coincide with almost every measured point.

If we could modify this initial model or use parts of it to obtain a similar one for Haynesville Shale, we could predict its velocities as well. Figure 6 is the comparison of initial model and the Haynesville measurements in terms of vertical P-wave velocity. It briefly tells us how the initial model differs from Haynesville Shale.
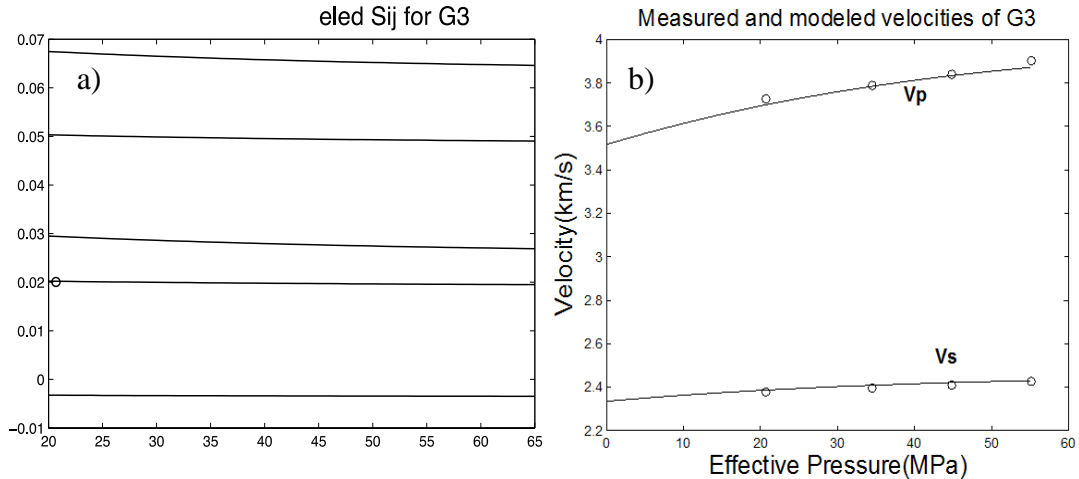

Figure 5. Compliance (a) and velocities (b) for both measurements (circles) and my initial model (solid lines) on brine saturated hard shale (sample G3 from Wang, 2002). The measured velocities are calculated from measured elastic components by Equations 1–4. The solid lines coincide with most circles in both figures.

Table 2. Best fitting parameters for initial model.

| S_{11}^{0} GPa^{-1}	S_{13}^{0} GPa^{-1}	S_{33}^{0} GPa^{-1}	S_{44}^{0} GPa^{-1}	S_{66}^{0} GPa^{-1}	SnBt	B	η	Pc MPa
0.0192	-0.00357	0.0258	0.0634	0.0485	1.837e-5	2	966	37
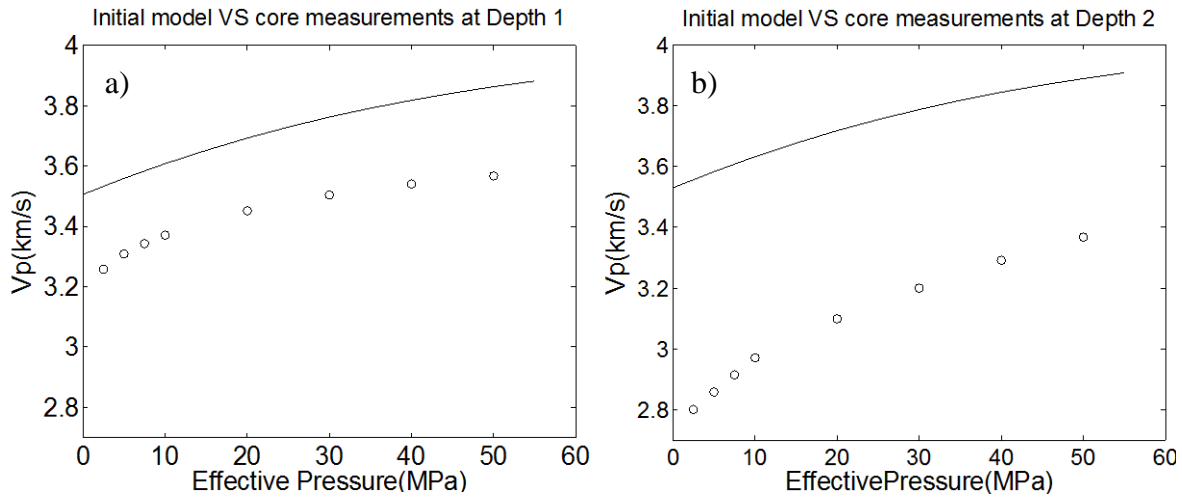
Figure 6. Model calculated velocity (solid lines) and lab measured velocity (black circles) comparison at normal propagation direction. The model used in both a) and b) is the initial model based on the analogous hard shale measurements. Black circles are brine substituted vertical P-wave velocity measurements. Compared to Figure 5b), it is clear that the initial model not fit Haynesville Shale.

Modified Model

From Equations 5–9, it's obvious that decreasing SnBt, Pc, η, and B will increase the compliance components. The increased compliances make the rock softer, and decrease velocity. Through many numerical experiments, we obtained the modified models that fitted the Haynesville Shale measurements. Figure 7 shows how these modified models fit the lab measurements. There are actually two set of models. The red line set fits measurements at low pressure, and the blue line set fits measurements at high pressure. These two model sets work over different pressure ranges because the mechanisms behind these two model sets are different. The velocities were measured on dry and not preserved cores. At low-pressure range, the increasing pressure closed most soft pores in the rock, which was an inelastic process. At high-pressure, the rock was deformed by increased pressure elastically. The in situ effective pressure of the Haynesville Shale is in the elastic range, so from here onward, I use only the elastic model (the blue line model set in Figure 7).

Modified model VS core measurements at Depth 1

Modified model VS core measurents at Depth 2
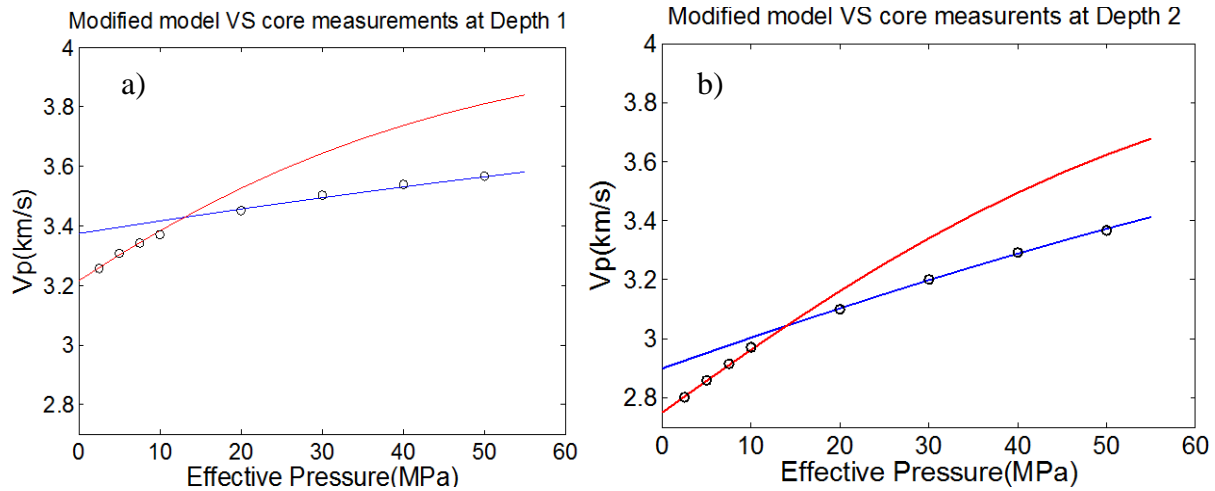
Figure 7. Modified model calculated velocity (solid lines) and lab measured velocity (black circles) comparison at normal propagation direction. The modified models at depth 1 (a)) and depth 2 (b)) are slightly deferent, but the major difference in velocity came from density difference. Black circles are same measurements as in Figure 6.

These modified models are not unique. For example, if we decreased B a little bit, then increasing η could compensate the difference in P-wave velocity caused by B. However, increasing the same amount for η could not compensate for S-wave velocity the same time. Owning to the shortage of S-wave measurements, we cannot tell which model fits the Haynesville Shale better.

Velocity prediction

From the modified model, we calculated the compliance components of Haynesville Shale (step 3) and then converted them back to stiffness components by Equations 15–19. Equations 1–4 gave the angle-dependent velocities (step 4). Figure 8 shows the three modes velocities as a function of propagation angle and effective pressure. P-wave and SH-wave velocity increase with propagation angle, whereas the SV-wave velocity increases at first and then decreases. The maximum SV-wave velocity occurs at approximately 40 degrees. In addition, all three modes velocities increase with effective pressure. A comparison of depth 1 series and depth 2 series shows that different depth samples have different velocity-angle and pressure dependent behavior although the velocity ranges are similar.
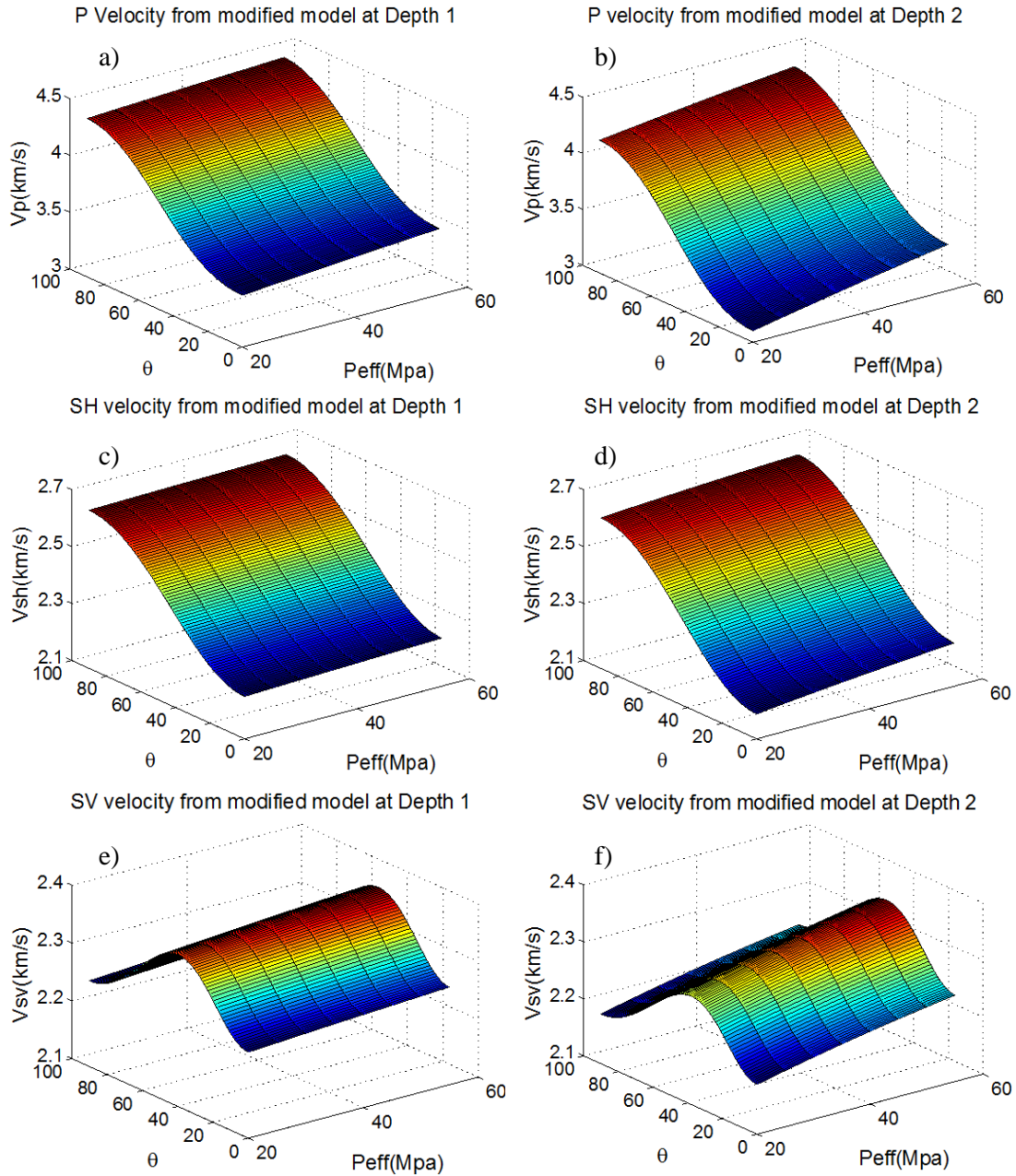
Figure 8. Velocity against propagation angle and effective pressure, colored in velocity. Velocities were calculated from modified models in Figure7. We used the elastic fitting models with pressure range 20 – 60Mpa. a), b) are P-wave velocity at depth 1 and depth 2. c), d) are horizontally polarized S-wave and e), f) are vertically polarized S-wave.

We selected a single slice of the models in Figure 8 along a constant pressure (Figure 9) to illustrate the angle-dependent velocity behavior clearer. The 40 MPa slice was chosen because the Haynesville Shale in situ effective pressure is approximately 45MPa - 55MPa.
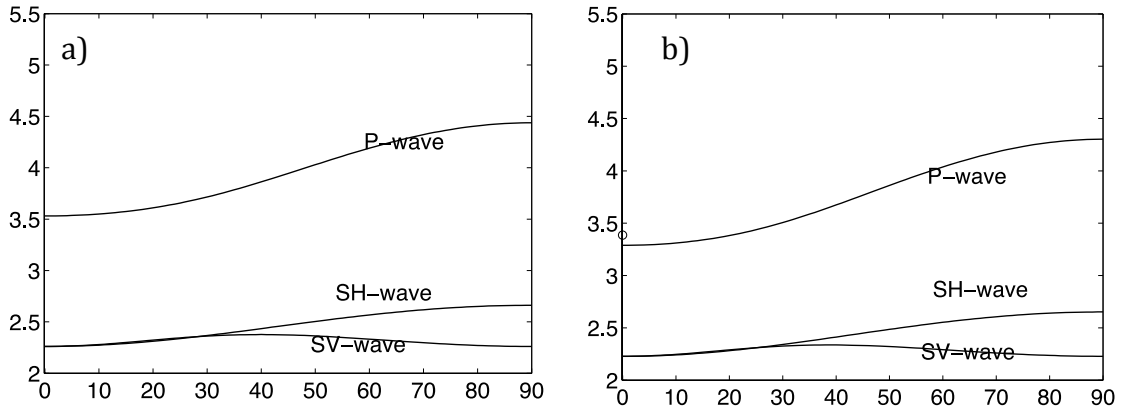
Figure 9. Velocity slice of Figure 8 from 40 MPa effective pressure. The angle-dependent velocity behavior is clearer in this figure.

UNCERTAINTY ESTIMATION

As mentioned in a previous section, in addition to the lab measurements, we also had P and S wave velocity well logs. Together with the Thomsen (1986) parameters $(\varepsilon, \gamma, \delta)$ from the same analogous shale sample used in initial model building, we generated reference velocities to estimate the uncertainty of predicted velocities from our model. From P and S wave velocity logs, we calculated the elastic constants C_{33} and C_{44}. Then the other three elastic components were calculated from Equations 20–22. The Thomsen parameters used here were derived from the G3 sample data at 40 MPa as listed in Table 1. Then by Equations 1–4, we calculated the three mode reference velocities (P, SH, and SV). These angle-dependent reference velocities are black solid lines in Figure 10.

$$\varepsilon = 2(C_{11} - C_{33})/2C_{33}, \tag{20}$$

$$\gamma = 2(C_{66} - C_{44})/2C_{44}, \tag{21}$$

$$\delta = \left[(C_{13} + C_{44})^2 - (C_{33} - C_{44})^2\right]/2C_{33}(C_{33} - C_{44}) \tag{22}$$

Reference velocities at zero-angle are the measured well log velocities. The difference between the predicted P-wave velocity and this P-wave log at the test locations was 3%. Compared to the reference velocity, the predicted P-wave results (blue lines) fell between 10% uncertainty over the propagation angles as shown in Figure 10. Magenta lines are the 10% uncertainty lines calculated form the predicted velocity. Unlike P-waves, S-wave velocities exhibited large deviations from the reference. Predicted S-wave velocities were higher than the

reference. This large difference can be associated both to the error of the reference and the lack of laboratory S-wave velocity measurements for the Haynesville Shale. In the reference velocities calculation, we assumed that Haynesville Shale had the same Thomsen parameters as the analogous hard shale sample. However, the comparison of analogous hard shale sample based initial model and Haynesville Shale lab measurements (Figure 6) illustrates the anisotropy property of these two shales are different. The size of this difference in terms of Thomsen parameters is unknown. On the other hand, the fitting model for pressure-dependent P-wave measurements is not unique. These models almost result in the same P-wave velocities, but different S-wave velocities. If pressure-dependent S-wave measurements were available, we could restrict these possibilities and reduce the uncertainty.
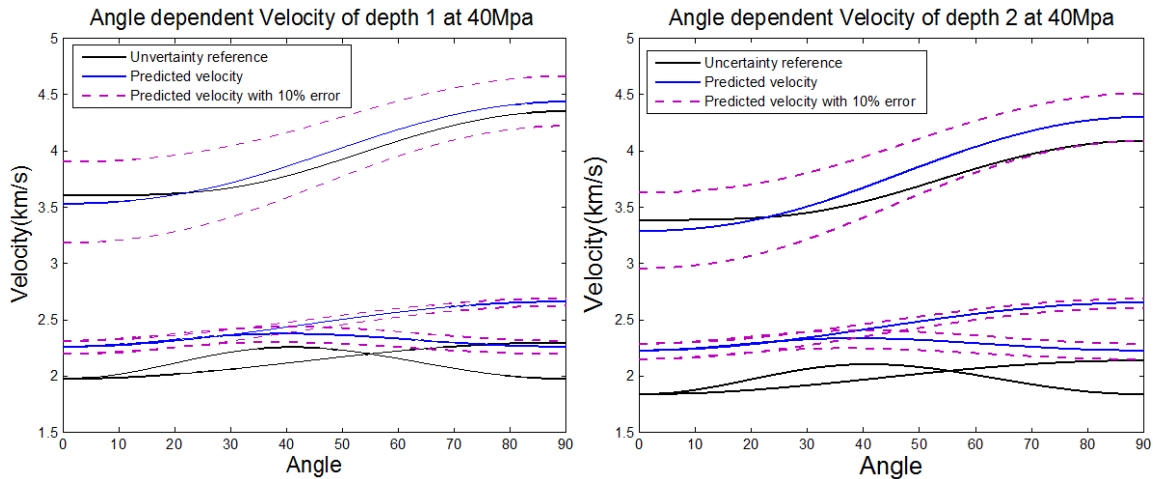
Figure 10. Uncertainty estimation. Blue lines are predicted velocities, and magenta dash lines are $\pm 10\%$ of them. The black lines are the reference velocities from the log data. High velocity sets of lines correspond to P-waves. The upper low velocity set of lines is the SH-wave, and the lowermost set corresponds to the SV-waves.

CONCLUSIONS

Shales exhibit anisotropy as a VTI system. Thus the propagation velocities through these rocks are angle-dependent. These angle-dependent velocities should be accounted for in anisotropic rock physics models. Therefore, predicting angle-dependent velocities is important in shale research. In this paper, we developed an integrated workflow to model the compliance tensor from pressure-dependent vertical P-wave velocity lab measurements and then predicted the velocities. The case study was from Haynesville Shale. Resulting P-wave and SH-wave velocity increased with propagation angle, whereas, SV-wave showed more complex behavior. Then I used the log data and analogous shale data to estimate the uncertainty. The differences

between P-wave velocity and sonic log velocity at sample locations are about 3%. Over the propagation angles, the estimated uncertainty was less than 10% for P-waves. As for S-waves, the uncertainty was much higher, but they showed the same angle-dependent variation trends. The S-wave uncertainty could be reduced if the S-wave measurements were available. Applying these results to field seismic data, we could reliably predict the angle-dependent P-wave velocity at the seismic scale. Importantly, an uncertainty estimate can be included with this prediction.

REFERENCES

Ciz R. and Shapiro, S. A., 2009, Stress-dependent anisotropy in transversely isotropic rocks: Comparison between theory and laboratory experiment on shale: Geophysics, **74**, 1, D7-D12, doi:10.1190/1.3008546.

Hart, B., Sayers, C., Jackson, A., 2011, An introduction to this special section: Shales: The Leading Edge, **30**, 272-273.

Hammes, U., Hamlin, H., Ewing, T., 2011, Geologic analysis of the Upper Jurassic Haynesville Shale in east Texas and west Louisiana: AAPG Bulletin, **95**, 10, 1643-1666.

Jones, L., Wang, H., 1981, Ultrasonic velocities in Cretaceous shales from the Williston basin: Geophysics, **46**, 3, 288-297.

Mavko, G., Mukerji, T., Dvorkin, J., 2009, *The Rock Physics Handbook: Tools for Seismic Analysis of Porous Media*. Cambridge University Press, Cambridge.

More, J. J., 1977, The Levenberg-Marquardt algorithm: Implementation and theory: Springer Verlag.

Pervukhina, M., Gurevich, B, and Golodoniuc, P., 2011, Parameterization of elastic stress sensitivity in shales: Geophysics, **76**, WA147.

Podio,A., 1968, Experimental determination of the dynamic elastic properties of anisotropic rocks – ultrasonic pulse method: Ph.D. Thesis, University of Texas at Austin, 8-30.

Thomsen, L., 1986 Weak elastic anisotropy: Geophysics, **51**, 1954-1966.

Vanorio, T., Mukerji, T., Mavko, G., 2008, Emerging methodologies to characterize the rock physics properties of organic-rich shales: The Leading Edge, **27**, 780-787.

Vernik, L., Nur, A., 1990, Ultrasonic velocity and anisotropy of pertroleum source rocks: the Bakken formation: SEG Technical Program Expanded Abstracts 1990, 845-848.

Vernik, L., Nur, A., 1992, Ultrasonic Velocity and Anisotropy of Pertroleum Source Rocks: Gephysics, **57**, 5, 727-735.

Wang, Z., 2002, Seismic anisotropy in sedimentary rocks, part 2: Laboratory data: Geophysics, **67**, 1423-1440.